

## Scanning Tunneling Microscopy of the $\pi$ Magnetism of a Single Carbon Vacancy in Graphene

Yu Zhang,<sup>1</sup> Si-Yu Li,<sup>1</sup> Huaqing Huang,<sup>2</sup> Wen-Tian Li,<sup>1</sup> Jia-Bin Qiao,<sup>1</sup> Wen-Xiao Wang,<sup>1</sup> Long-Jing Yin,<sup>1</sup> Ke-Ke Bai,<sup>1</sup> Wenhui Duan,<sup>2</sup> and Lin He<sup>1,\*</sup>

<sup>1</sup>*Center for Advanced Quantum Studies, Department of Physics, Beijing Normal University, Beijing 100875, People's Republic of China*

<sup>2</sup>*State Key Laboratory of Low-Dimensional Quantum Physics and Collaborative Innovation Center of Quantum Matter, Department of Physics, Tsinghua University, Beijing 100084, People's Republic of China*

(Received 4 May 2016; published 10 October 2016)

Pristine graphene is strongly diamagnetic. However, graphene with single carbon atom defects could exhibit paramagnetism. Theoretically, the  $\pi$  magnetism induced by the monovacancy in graphene is characteristic of two spin-split density-of-states (DOS) peaks close to the Dirac point. Since its prediction, many experiments have attempted to study this  $\pi$  magnetism in graphene, whereas only a notable resonance peak has been observed around the atomic defects, leaving the  $\pi$  magnetism experimentally elusive. Here, we report direct experimental evidence of  $\pi$  magnetism by using a scanning tunneling microscope. We demonstrate that the localized state of the atomic defects is split into two DOS peaks with energy separations of several tens of meV. Strong magnetic fields further increase the energy separations of the two spin-polarized peaks and lead to a Zeeman-like splitting. Unexpectedly, the effective  $g$  factor around the atomic defect is measured to be about 40, which is about 20 times larger than the  $g$  factor for electron spins.

DOI: 10.1103/PhysRevLett.117.166801

According to Lieb's theorem, derived for a half-filled single-band Hubbard model, the ground state of materials with a bipartite lattice has a magnetic moment  $|N_A - N_B|\mu_B$ , where  $N_A$  and  $N_B$  are the numbers of sublattice sites [1]. Graphene has a unique bipartite honeycomb lattice (the two sublattices are denoted by  $A$  and  $B$ ). Therefore, a single carbon atom vacancy in graphene is expected to lead to a magnetic moment [2–10]. First principles calculations predicted that an isolated vacancy in graphene with a planar configuration has a local magnetic moment of  $1.5\mu_B$ , in which  $1\mu_B$  contributed by the dangling  $\sigma$  states and about  $0.5\mu_B$  contributed by  $\pi$  electrons [2,11,12]. The  $\pi$  magnetism in graphene is closely linked to two spin-split density-of-states (DOS) peaks near the Dirac point [2,11,12], which enable us to directly detect the signature of  $\pi$  magnetism on individual monovacancy by investigating its electronic structure. Very recently, the emergence of edge magnetism in an individual zigzag graphene nanoribbon is also studied by measuring its electronic structure via a scanning tunneling microscope (STM) [13–15].

To create atomic vacancies, the graphene systems were usually irradiated with high-energy ions [7–10] because the formation energy of a single atom vacancy in graphene is as high as about 7.4 eV [16,17]. Unfortunately, only a profound resonance peak has been observed on the irradiated vacancies [7–10]. The quenching of the magnetic moment of monovacancy in graphene is partially attributed to the graphene-substrate interaction [9]. Theoretically, a monovacancy in graphene with a metastable nonplanarity

configuration is predicted to have a vanishing magnetic moment and the metastable configuration is only 50–100 meV above the ground state (i.e., the planar configuration) [9,12]. These irradiated vacancies generated by high-energy ions may not be in the ground state. Therefore, the possible graphene-substrate interaction and the existence of the metastable configuration make the  $\pi$  magnetism of monovacancy in graphene quite elusive. In the current work, we directly synthesize graphene with a high density of monovacancies on Rh foils using a facile ambient pressure chemical vapor deposition (CVD) method (more details are given in below and in Fig. S1 of the Supplemental Material [18]) [22–24]. We demonstrate here, using the STM measurements, that the studied monovacancies are in the planar configuration. The spatial-resolved scanning tunneling spectroscopy (STS) spectra and the ground-state planar configuration of the monovacancies provide us unprecedented opportunities to directly measure the two spin-split DOS peaks of the  $\pi$  magnetism in graphene.

Figure 1(a) shows Raman spectroscopy mapping of a graphene multilayer on Rh foil. The regions with different colors reflect a change in the intensity of the Raman D peak (see Fig. S2 of the Supplemental Material [18]), i.e., the density of defects in graphene [25]. The existence of high density of atomic-scale defects in graphene on Rh foil is further confirmed by the STM measurements. Figure 1(b) shows a representative STM image of the studied graphene and tens of atomic-scale defects can be clearly identified. Such a high density of defects is attributed to a segregation

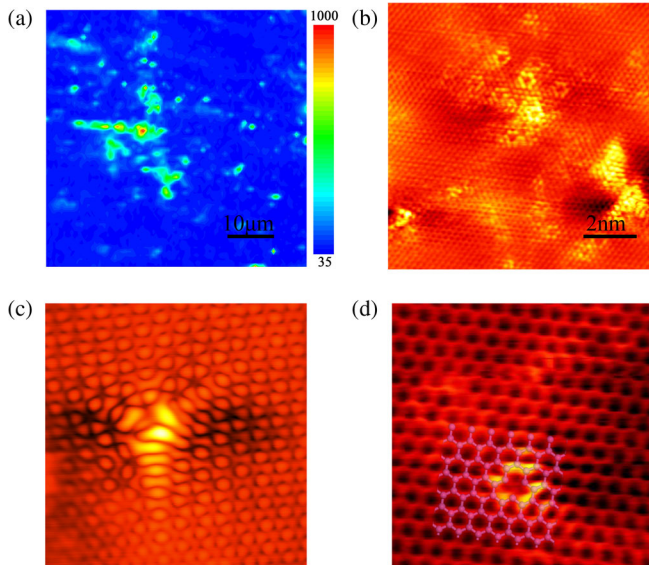


FIG. 1. Graphene with atomic defects on a Rh foil. (a)  $46\ \mu\text{m} \times 46\ \mu\text{m}$  Raman mapping of the  $D$  band (peak at  $1350\ \text{cm}^{-1}$  of Raman spectrum) of graphene on Rh foil. (b)  $10\ \text{nm} \times 10\ \text{nm}$  STM topographic image of graphene region with high density of defects on Rh foil. (c) Atomic resolution STM image of a single carbon vacancy in the topmost graphene sheet. (d) Zoom-in STM image of a single carbon vacancy in the underlying graphene. The atomic structure of graphene with a single carbon vacancy is overlaid onto the STM image to determine the position of the vacancy.

mechanism for the graphene grown on Rh foil and the high carbon solubility of this metal [24]. In the STM measurements, the single carbon vacancies of graphene exhibit two distinct topographic signatures, as shown in Figs. 1(c) and 1(d). For the single carbon vacancy on the topmost graphene layer, we observe the triangular  $\sqrt{3} \times \sqrt{3}R30^\circ$  interference pattern (Fig. 1(c) and Fig. S3 of the Supplemental Material [18]), which is similar to that reported in previous studies [6–9]. Electronic contributions dominate the STM contrast near the monovacancy, making it difficult to resolve its atomic structure. However, it is still possible to determine the position of the monovacancy by overlaying the atomic structure of graphene with a single carbon vacancy onto the STM image, as shown in Fig. S5 of the Supplemental Material [18]. For the single carbon vacancy on the underlying graphene, the topmost graphene sheet reduces the contributions of electronic DOS to the STM contrast and close-up topographic studies of such a defect could directly reveal its atomic structure, as shown in Fig. 1(d). STM measurements at varying voltage bias show unblemished atomically resolved honeycomb structure of the topmost graphene layer above the single carbon vacancy (Fig. S4 of the Supplemental Material [18]). This confirms that the defect in Fig. 1(d) is on the underlying graphene. There are other types of atomic defects—such as adatoms, interstitial atoms, substitutional atoms, and large

voids—in graphene (see Fig. S5 of the Supplemental Material [18]). However, they exhibit quite different features in the STM measurements comparing to that of single carbon vacancy. For example, it is easy to distinguish the large voids and the single carbon vacancy by examining their atomic-resolution STM images. The existence of a little Jahn-Teller distortion [2,26] around the single carbon vacancy also ensures us to exclude adatoms or interstitial atoms as the origin of the triangular patterns in our STM images (Fig. 1(c)). In our experiment, we used methane vapor to synthesize the graphene system, which allows us to completely exclude the emergence of high density of substitutional atoms in our sample (see the Supplemental Material [18] for details of discussion). Therefore, we can rule out all these scenarios as the origin of the observed features in our STM images (Fig. 1 and Figs. S3 and S4 of the Supplemental Material [18]) and conclude that we synthesized graphene with high density of monovacancies using a facile CVD method.

According to theoretical calculations, the single unpaired C atom of the monovacancy in graphene with the metastable nonmagnetic configuration is about 50 pm out of the graphene plane [9,12]. To confirm that the studied single carbon vacancies are not in the nonmagnetic configuration, we use different bias voltages to acquire the STM images of the defects on the topmost layer (Fig. S6 of the Supplemental Material [18]). The height of the vacancy depends strongly on the bias, showing that the STM contrast originates primarily from the locally modified electronic structure rather than from topographic features. The structural origin of observed protrusions of the vacancies is estimated to be less than 20 pm. For the graphene multilayer grown on Rh foil, there is usually rotational misalignment between the layers, resulting in moiré patterns in STM images (Fig. S7 of the Supplemental Material [18]) [22,23]. In such a case, the topmost graphene sheet usually decouples from the underlying graphene systems and the Landau quantization of massless Dirac fermions can be observed in the decoupled topmost graphene sheet [27–32], as demonstrated in Fig. 3. Therefore, we can also exclude any possible interaction between the single carbon vacancy and the substrate.

Figure 2(a) shows several representative spectra recorded around a single carbon vacancy in graphene on Rh foil. With approaching the monovacancy, a resonance peak emerges in the tunneling spectra, which is similar to that reported in previous studies [7–10]. A notable feature of the STS spectra is the splitting of the resonance peak within  $\sim 0.6\ \text{nm}$  around the vacancy and its sensitive dependency on the recorded positions. The tunneling spectrum gives direct access to the local DOS of the surface beneath the STM tip. The two peaks of the STS spectra are attributed to the DOS of two spin-split states and their amplitudes reflect the distribution of the electron spin density around the defect. Similar observations are obtained in tens of single

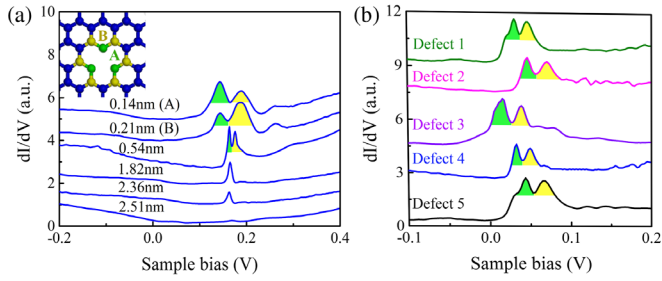


FIG. 2. Spin-split states of single carbon vacancy in graphene. (a) STS spectra recorded at different distances away from a single carbon vacancy. The two peaks reflect the DOS with opposite spin polarizations. Inset: Schematic structure of a single carbon vacancy. The first and second spectra are measured on the nearest-neighbor and the next-nearest-neighbor of the monovacancy. (b) Representative STS spectra of five different monovacancies. The energy separations of the two peaks  $\Delta E$  vary from about 20 to about 60 meV.

carbon vacancies in the graphene on Rh foils with many STM tips, and Figure 2(b) shows several typical spectra of five different monovacancies in our studies. The appearance of two spin-split states reminds us of the characteristics of the  $\pi$  magnetism in the single carbon vacancy of graphene [2].

Very recently, similar two spin-split states are observed around isolated hydrogen atoms absorbed on graphene and are attributed to the emergence of magnetism in graphene [33]. In their experiment, the two spin-polarized states appear only when the localized states induced by hydrogen absorption are localized at the Fermi energy and they vanish when the system is either  $n$ - or  $p$ -type doping [33]. Whereas, the two spin-polarized states observed in our experiment are quite robust even when their energies are shifted away from the Fermi level (in our experiment, the two states are located above the Fermi level  $\sim 100$  meV due to charge transfer between graphene and the substrate), as shown in Fig. 2. Our first principles calculations also

indicate that the splitting of the vacancy-induced graphene state still exists in both  $n$ - and  $p$ -types doping graphene (Figs. S8 and S9 of the Supplemental Material [18]). This is quite different from the magnetism of graphene induced by hydrogen absorption [33], which is sensitive to the doping and, therefore, may be problematic in typical graphene devices toward realizing robust magnetic graphene for applications. The  $\pi$  magnetism of the single carbon vacancies is expected to be observed when there is an imbalance for the occupation of the split states. Our result, as shown in Fig. 2(a), indicates that the spin splitting is much more localized than the resonance peak of the single carbon vacancy. The two spin-polarized peaks merge into a single one at  $\sim 0.6$  nm away from the monovacancy, implying that electron-electron interactions of the localized states play a vital role in the spin splitting (with approaching the monovacancy, the intensity of the localized states increases dramatically). Such a feature has not been revealed in previous first principles calculations and further theoretical calculations by taking into account the electron-electron interactions are needed to fully reproduce the experimental observation.

To further explore the electronic properties of the single carbon vacancies in graphene on Rh foils, we carried out STS measurements in various magnetic fields. Figure 3(a) shows spectra recorded in high magnetic fields at position  $\sim 2.6$  nm away from the defect. The spectra exhibit Landau quantization of massless Dirac fermions and the energies of the discrete Landau levels (LL) can be described by [31,32,34,35]

$$E_n = \text{sgn}(n) \sqrt{2e\hbar v_F^2 |n| B} + E_0, \quad (1)$$

$$n = \dots - 2, -1, 0, 1, 2, \dots$$

Here,  $E_0$  is the energy of Dirac point,  $e$  is the electron charge,  $n$  is the Landau index,  $\hbar$  is the Planck's constant, and  $v_F$  is the Fermi velocity. The observation of a sequence

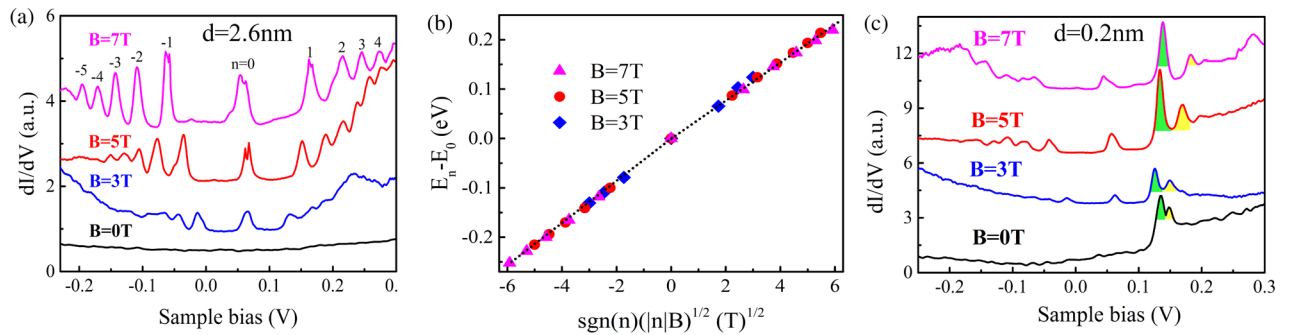


FIG. 3. Landau quantization around the monovacancy in graphene. (a) Tunneling spectra recorded at position 2.6 nm away from a monovacancy under different magnetic fields. LL peak indices are labeled and the data are offset in the Y axis for clarity. A slight splitting of  $LL_0$  and  $LL_{\pm 1}$  can be observed in the field of 7 T. (b) The energies of LLs show a linear dependence against  $\text{sgn}(n)(|n|B)^{1/2}$ , as expected for massless Dirac fermions in the graphene monolayer. The dashed curves are linear fits of the data with Eq. (1). (c) Tunneling spectra recorded at position  $\sim 0.2$  nm away from the monovacancy under various magnetic fields. The energy separations of the two peaks increase with the magnetic fields.

of LLs showing single-layer-graphene scaling demonstrates the efficient decoupling of the topmost graphene sheet from the supporting substrate. The linear fit of the experimental data to Eq. (1), as shown in Fig. 3(b), yields the Fermi velocity of electrons  $v_F^e = 1.18 \times 10^6$  m/s and the velocity of holes  $v_F^h = 1.04 \times 10^6$  m/s. Such a large electron-hole asymmetry may arise from the local lattice deformation around the monovacancy and the electron scattering of the charged defect [36,37].

Besides the large electron-hole asymmetry, the other notable observation of the spectra is the lifting of the degeneracy of LLs in high magnetic fields, as shown in Fig. 3(a). For example, the energy splitting of the  $LL_0$  is about 5.5 meV in the field of 5 T and it increases to about 8.8 meV in the field of 7 T. Similar energy splits are also observed in  $LL_{-1}$  and  $LL_1$  in the field of 7 T. The energy splitting of LLs with higher orbital indices is not observed in our experiment because the linewidth of LLs increases with energy. Such a behavior is related to the quasiparticle lifetimes, which decrease with the energy difference from the Fermi level [29,31]. Fitting the splitting energies of the  $LL_0$  to a Zeeman-like dependence,  $E = g\mu_B B$ , yields the  $g$  factor  $g \sim 21$ . We attribute this energy splitting to the lifting of the valley degeneracies because the effective  $g$  factor of the valley splitting in graphene is measured to be about 18.4 [31]. In the presence of high magnetic field, the electrons are spatially more localized and the electron-electron interaction is expected to be enhanced. The enhanced interaction lifts LL degeneracies and generates gaps in graphene [31,38]. The observation of interaction-driven gaps, which increase with the magnetic fields, is a clear signature that the electron-electron interaction in graphene is enhanced with increasing the fields.

Figure 3(c) shows several representative spectra recorded in high magnetic fields at a monovacancy. We can detect weak signals of LLs at the monovacancy because the wave functions of LLs have their spatial extent,  $\sim 2\sqrt{N}l_B$  (here  $N$  is the Landau index and  $l_B = \sqrt{\hbar/eB}$ , which is of the order of 10 nm for the magnetic fields applied in our experiment). A notable result of the spectra is that the energy separations of the two spin-polarized DOS peaks of the monovacancy increase with the magnetic fields, as shown in Fig. 3(c) and summarized in Fig. 4. This demonstrated explicitly that the two peaks in the STS spectra are the predicted two spin-polarized DOS peaks, which are closely related to the  $\pi$  magnetism of single carbon vacancy in graphene. A linear fit the experimental data to  $\Delta E = g^*\mu_{\text{eff}}B$  yields  $g^* \sim 40$  (here we use  $\mu_{\text{eff}} \sim 1.5\mu_B$ ). This effective  $g$  factor is much larger than that of the valley splitting measured away from the defect, implying a significant contribution of the monovacancy to the giant enhancement. Previously, a large effective  $g$  factor of  $g \sim 34$  had been observed in electron puddles of graphene bilayer on  $\text{SiO}_2$  substrate, and such a large  $g$  factor is attributed to many-body

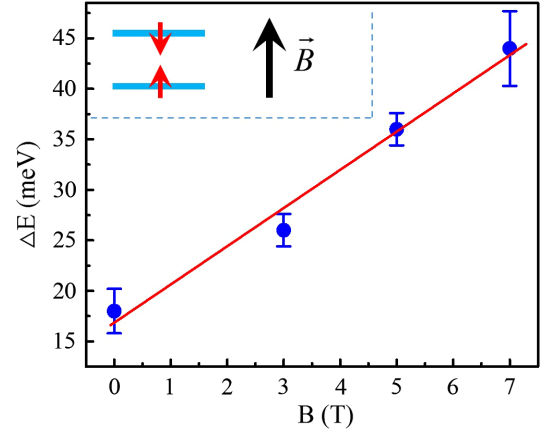


FIG. 4. Energy separations of the two spin-split peaks of the monovacancy as a function of magnetic fields. A linear fit of the energy separations versus magnetic field yields an effective  $g$  factor of 40 around the monovacancy. Inset: schematic of the energy level split of the two spin-split states in high magnetic fields.

interactions [38]. In our case, the spin splitting of the two peaks of the monovacancy in graphene is determined by the strength of the electron-electron interaction. Thus, the enhanced interaction in high fields further increases the energy separations of the two spin-polarized peaks. We believe that the observed large  $g$  factor in our experiment is due in part to the strong spin polarization of electron density of the monovacancy, and in part to the enhanced electron-electron interactions in high magnetic fields.

In summary, we demonstrate that the single carbon vacancy in graphene induces  $\pi$  magnetism characterized by two spin-polarized states and we show that the splitting of the vacancy-induced graphene state is quite robust in both  $n$ - and  $p$ -types doping graphene. This may raise hopes of graphene-based next-generation information technologies.

We thank Professor Ji Feng, Professor Zhe Yuan, Professor Fan Zhang, and Professor Haiwen Liu for helpful discussions. This work was supported by the National Basic Research Program of China (Grants No. 2014CB920903 and No. 2013CBA01603), the National Natural Science Foundation of China (Grants No. 11674029, No. 11422430, No. 11374035, and No. 11334006), the program for New Century Excellent Talents in University of the Ministry of Education of China (Grant No. NCET-13-0054). L.H. also acknowledges support from the National Program for Support of Top-notch Young Professionals.

Y.Z. and S-Y.L. contributed equally to this work.

*Note added.*—Recently, we became aware of the work of Gonzalez-Herrero *et al.* [33], which showed the existence of magnetism in graphene by using hydrogen atoms.

- \*To whom all correspondence should be addressed.  
helin@bnu.edu.cn
- [1] E. H. Lieb, Two Theorems on the Hubbard Model, *Phys. Rev. Lett.* **62**, 1201 (1989).
  - [2] O. V. Yazyev and L. Helm, Defect-induced magnetism in graphene, *Phys. Rev. B* **75**, 125408 (2007).
  - [3] O. V. Yazyev, Emergence of magnetism in graphene materials and nanostructures, *Rep. Prog. Phys.* **73**, 056501 (2010).
  - [4] K. M. McCreary, A. G. Swartz, W. Han, J. Fabian, and R. K. Kawakami, Magnetic Moment Formation in Graphene Detected by Scattering of Pure Spin Currents, *Phys. Rev. Lett.* **109**, 186604 (2012).
  - [5] R. R. Nair, M. Sepioni, I-Ling Tsai, O. Lehtinen, J. Keinonen, A. V. Krasheninnikov, T. Thomson, A. K. Geim, and I. V. Grigorieva, Spin-half paramagnetism in graphene induced by point defects, *Nat. Phys.* **8**, 199 (2012).
  - [6] R. R. Nair, I.-L. Tsai, M. Sepioni, O. Lehtinen, J. Keinonen, A. V. Krasheninnikov, A. H. Castro Neto, M. I. Katsnelson, A. K. Geim, and I. V. Grigorieva, Dual origin of defect magnetism in graphene and its reversible switching by molecular doping, *Nat. Commun.* **8**, 2010 (2013).
  - [7] W. Han, R. K. Kawakami, M. Gmitra, and J. Fabian, Graphene spintronics, *Nat. Nanotechnol.* **9**, 794 (2014).
  - [8] M. M. Ugeda, I. Brihuega, F. Guinea, and J. M. Gómez-Rodríguez, Missing Atom as a Source of Carbon Magnetism, *Phys. Rev. Lett.* **104**, 096804 (2010).
  - [9] M. M. Ugeda, D. Fernández-Torre, I. Brihuega, P. Pou, A. J. Martínez-Galera, Rubén Pérez, and J. M. Gómez-Rodríguez, Point Defects on Graphene on Metals, *Phys. Rev. Lett.* **107**, 116803 (2011).
  - [10] J. Mao, Y. Jiang, D. Moldovan, G. Li, K. Watanabe, T. Taniguchi, M. R. Masir, F. M. Peeters, and E. Y. Andrei, Realization of a tunable artificial atom at a supercritically charged vacancy in graphene, *Nat. Phys.* **12**, 545 (2016).
  - [11] B. R. K. Nanda, M. Sherafati, Z. Popović, and S. Satpathy, Electronic structure of the substitutional vacancy in graphene: density-functional and Green's function studies, *New J. Phys.* **14**, 083004 (2012).
  - [12] H. Padmanabhan and B. R. K. Nanda, Intertwined lattice deformation and magnetism in monovacancy graphene, *Phys. Rev. B* **93**, 165403 (2016).
  - [13] C. Tao, L. Jiao, O. V. Yazyev, Y.-C. Chen, J. Feng, X. Zhang, R. B. Capaz, J. M. Tour, A. Zettl, S. G. Louie, H. Dai, and M. F. Crommie, Spatially resolving edge states of chiral graphene nanoribbons, *Nat. Phys.* **7**, 616 (2011).
  - [14] Y. Y. Li, M. X. Chen, M. Weinert, and L. Li, Direct experimental determination of onset of electron-electron interactions in gap opening of zigzag graphene nanoribbons, *Nat. Commun.* **5**, 4311 (2014).
  - [15] Gabor Zsolt Magda, Xiaozhan Jin, Imre Hagymasi, Peter Vancso, Zoltan Osvath, Peter Nemes-Incze, Chanyong Hwang, Laszlo P. Biro, and Levente Tapasztó, Room-temperature magnetic order on zigzag edges of narrow graphene nanoribbons, *Nature (London)* **514**, 608 (2014).
  - [16] A. A. El-Barbary, R. H. Telling, C. P. Ewels, M. I. Heggie, and P. R. Briddon, Structure and energetics of the vacancy in graphite, *Phys. Rev. B* **68**, 144107 (2003).
  - [17] P. O. Lehtinen, A. S. Foster, Yuchen Ma, A. V. Krasheninnikov, and R. M. Nieminen, Irradiation-Induced Magnetism in Graphite: A Density Functional Study, *Phys. Rev. Lett.* **93**, 187202 (2004).
  - [18] See Supplemental Material at <http://link.aps.org/supplemental/10.1103/PhysRevLett.117.166801> for methods, more STM images, STS spectra, and details of the analysis, which includes Refs. [19–21].
  - [19] K.-K. Bai, Y. Zhou, H. Zheng, L. Meng, H. Peng, Z. Liu, J.-C. Nie, and L. He, Creating One-dimensional Nanoscale Periodic Ripples in a Continuous Mosaic Graphene Monolayer, *Phys. Rev. Lett.* **113**, 086102 (2014).
  - [20] G. Kresse and J. Furthmüller, Efficiency of ab-initio total energy calculations for metals and semiconductors using a plane-wave basis set, *Comput. Mater. Sci.* **6**, 15 (1996).
  - [21] J. P. Perdew, K. Burke, and M. Ernzerhof, Generalized Gradient Approximation Made Simple, *Phys. Rev. Lett.* **77**, 3865 (1996).
  - [22] W. Yan, M. Liu, R.-F. Dou, L. Meng, L. Feng, Z.-D. Chu, Y. Zhang, Z. Liu, J.-C. Nie, and L. He, Angle-dependent van Hove Singularities in a Slightly Twisted Graphene Bilayer, *Phys. Rev. Lett.* **109**, 126801 (2012).
  - [23] W. Yan, W.-Y. He, Z.-D. Chu, M. Liu, L. Meng, R.-F. Dou, Y. Zhang, Z. Liu, J.-C. Nie, and L. He, Strain and curvature induced evolution of electronic band structures in twisted graphene bilayer, *Nat. Commun.* **4**, 2159 (2013).
  - [24] H. Yan, C.-C. Liu, K.-K. Bai, X. Wang, M. Liu, W. Yan, L. Meng, Y. Zhang, Z. Liu, J.-C. Nie, Y. Yao, and L. He, Electronic structures of graphene layers on a metal foil: the effect of atomic-scale defects, *Appl. Phys. Lett.* **103**, 143120 (2013).
  - [25] A. C. Ferrari, J. C. Meyer, V. Scardaci, C. Casiraghi, M. Lazzeri, F. Mauri, S. Piscanec, D. Jiang, K. S. Novoselov, S. Roth, and A. K. Geim, Raman Spectrum of Graphene and Graphene Layers, *Phys. Rev. Lett.* **97**, 187401 (2006).
  - [26] Yuchen Ma, P. O. Lehtinen, A. S. Foster, and R. M. Nieminen, Magnetic properties of vacancies in graphene, and single-walled carbon nanotubes, *New J. Phys.* **6**, 68 (2004).
  - [27] W. Yan, L. Meng, M. Liu, J.-B. Qiao, Z.-D. Chu, R.-F. Dou, Z. Liu, J.-C. Nie, D. G. Naugle, and L. He, Angle-dependent van Hove singularities and their breakdown in twisted graphene bilayers, *Phys. Rev. B* **90**, 115402 (2014).
  - [28] G. Li, A. Luican, and E. Y. Andrei, Scanning Tunneling Spectroscopy of Graphene on Graphite, *Phys. Rev. Lett.* **102**, 176804 (2009).
  - [29] A. Luican, G.-H. Li, A. Reina, J. Kong, R. R. Nair, K. S. Novoselov, A. K. Geim, and E. Y. Andrei, Single-Layer Behavior and Its Breakdown in Twisted Graphene Layers, *Phys. Rev. Lett.* **106**, 126802 (2011).
  - [30] L.-J. Yin, H. Jiang, J.-B. Qiao, and L. He, Direct imaging of topological edge states at a bilayer graphene domain wall, *Nat. Commun.* **7**, 11760 (2016).
  - [31] Y. J. Song, A. F. Otte, Y. Kuk, Y. Hu, D. B. Torrance, P. N. First, W. A. D. Heer, H. Min, S. Adam, M. D. Stiles, A. H. MacDonald, and J. A. Stroscio, High-resolution tunnelling spectroscopy of a graphene quartet, *Nature (London)* **467**, 185 (2010).
  - [32] D. L. Miller, K. D. Kubista, G. M. Rutter, M. Ruan, W. A. D. Heer, P. N. First, and J. A. Stroscio, Observing the quantization of zero mass carriers in graphene, *Science* **324**, 924 (2009).

- [33] H. Gonzalez-Herrero, J. M. Gomez-Rodriguez, P. Mallet, M. Moaied, J. J. Palacios, C. Salgado, M. M. Ugeda, J.-Y. Veuillen, F. Yndurain, and I. Brihuega, Atomic-scale control of graphene magnetism by using hydrogen atoms, *Science* **352**, 437 (2016).
- [34] L.-J. Yin, S.-Y. Li, J.-B. Qiao, J.-C. Nie, and L. He, Landau quantization in graphene monolayer, Bernal bilayer, and Bernal trilayer on graphite surface, *Phys. Rev. B* **91**, 115405 (2015).
- [35] L.-J. Yin, J.-B. Qiao, W.-J. Zuo, W.-T. Li, and L. He, Experimental evidence for non-Abelian gauge potentials in twisted graphene bilayers, *Phys. Rev. B* **92**, 081406(R) (2015).
- [36] K.-K. Bai, Y.-C. Wei, J.-B. Qiao, S.-Y. Li, L.-J. Yin, W. Yan, J.-C. Nie, and L. He, Detecting giant electron-hole asymmetry in a graphene monolayer generated by strain and charged-defect scattering via Landau level spectroscopy, *Phys. Rev. B* **92**, 121405(R) (2015).
- [37] S.-Y. Li, K.-K. Bai, L.-J. Yin, J.-B. Qiao, W.-X. Wang, and L. He, Observation of unconventional splitting of Landau levels in strained graphene, *Phys. Rev. B* **92**, 245302 (2015).
- [38] G. M. Rutter, S. Jung, N. N. Klimov, D. B. Newell, N. B. Zhitenev, and J. A. Stroscio, Microscopic polarization in bilayer graphene, *Nat. Phys.* **7**, 649 (2011).